Experimental Evaluation of the Planar Assumption in Magnetic Positioning

David Hanley[1], Xiangyuan Zhang[1], Augusto S. Dantas de Oliveira[2], Daniel Steinberg[2], and Timothy Bretl[2]
Department of Electrical and Computer Engineering[1]
Department of Aerospace Engineering[2]
University of Illinois at Urbana-Champaign
Email: {hanley6,xz7,dantasd2,dshtey2,tbretl}@illinois.edu

***Abstract*—In this paper, we confirm the hypothesis that the magnetic field inside a building can vary significantly as a function of height. We collected data with twenty magnetometers spaced evenly from knee height to head height and mounted to a ground robot, which we drove through two different buildings on the campus of the University of Illinois at Urbana-Champaign. We applied Gaussian process regression to build a map of the magnetic field at each height. We compared these maps and saw pairwise differences of more than $1\ \mu T$ in up to 20% of each test environment, a threshold that we argue would prevent meeting the requirements of common indoor positioning applications. These results call into question the planar assumption that is commonly made when deriving methods of indoor positioning that are based on the use of magnetic fields.**

***Index Terms*—Magnetic Localization, Indoor Localization, Magnetic Fields, Three-Dimensional Magnetic Field Analysis**

I. Introduction

Methods of indoor positioning that are based on the use of magnetic fields typically assume that these magnetic fields do not vary with height [1]–[11]. This assumption is known to be reasonable when the magnetic sensor is approximately halfway between floor and ceiling in a building made only of vertically oriented magnetic beams [12]. However, buildings are made up of more than vertically oriented beams, and sensor height can be well outside this range, depending on who (or what) is carrying the sensor and on how it is being held (Figure 1). The extent of the resulting variation in magnetic field strength and the impact of this variation on positioning accuracy cannot be derived from existing datasets, most of which have been generated either by taking measurements at a constant height or by aggregating all measurements, regardless of height [13]–[15]. International standards for test and evaluation of indoor positioning methods are consistent with these existing datasets—they do not currently require changes in sensor height with respect to a previously generated map, and so also ignore the possible impact of the resulting magnetic field variation on positioning accuracy [16].

In this paper, we confirm the hypothesis that the magnetic field inside a building can vary significantly as a function of height. We also show that, as a consequence of these variations, localization and mapping requirements may be left unachieved. This is particularly true when ground robots, like the Clearpath Jackal robot shown in Figure 1, localize using the same magnetic map as a pedestrian.

978-1-5386-5635-8/18/$31.00 © 2018 IEEE

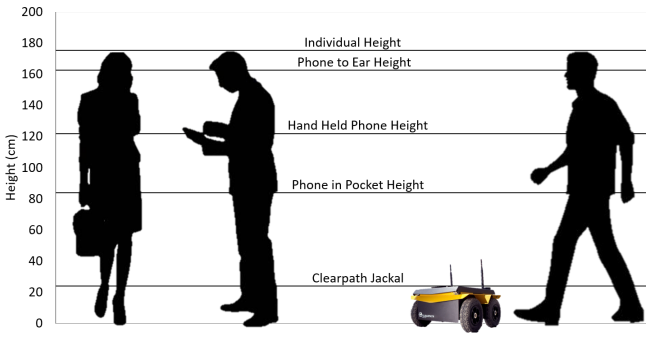

Fig. 1. The approximate height of magnetometers on a phone held to the ear, held in the hand during texting, and in a pocket. We also show the height of a Clearpath Jackal robot.

While the planar assumption in magnetic positioning currently appears quite ubiquitous, there is some prior work that does not use this assumption. This work does not test our hypothesis. Moreover, none of the results presented from prior tests can be used to confirm or reject our hypothesis. Akai and Ozaki sought to efficiently create maps for three dimensional magnetic fields [17]. Most description of methodology and results in their work show the effectiveness of using their approach to Gaussian process regression through images. But these results do not enable one to conclude how effective or ineffective the planar assumption is at different heights. The magnetic field of a building was modelled in three dimensions to calibrate and measure satellite magnetic sources by Yamazaki et al [18]. Results here are presented at heights more than 8.6 meters apart. A magneto-visual-inertial odometry algorithm has also been developed under the assumption that a magnetic field varies in three dimensions [19]. In this work, results are presented in terms of positioning error of the magneto-visual-inertial odometry system, which we cannot use to draw direct conclusions about the planar assumption.

We define the meaning of "significant variations of a magnetic field with respect to height" in Section II. We justify our hypothesis for a simple, analytically tractable case study in Section III. We then collect data of the magnetic field

TABLE I
REQUIREMENTS FOR POSITIONING

Number	Scenario	Positioning Requirement	Threshold
(1)	BVI Assistant	$< 2\ m$	$1\ \mu T$
(2)	Retail Semantics	$< 0.2\ m$ mean	$1\ \mu T$

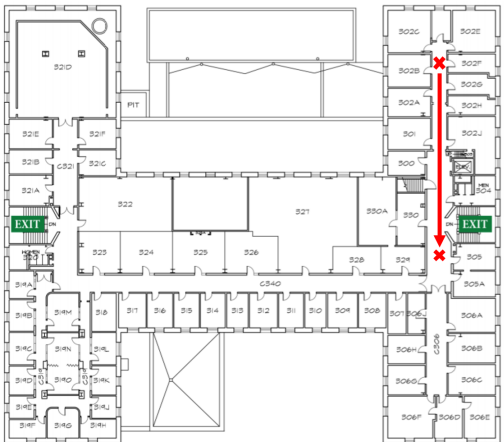

Fig. 2. The floor plan of the third floor of Talbot Laboratory used in the MagPIE dataset. The approximate path used for the test is shown.

at twenty different heights in two different buildings at the University of Illinois at Urbana-Champaign. Each magnetometer is separated vertically by three inches (approximately one standard deviation of the height of men and women) [20]. We describe this methodology in detail in Section IV. We test our hypotheses with respect to maps generated with Gaussian process regression (GPR) in Section V. We present conclusions and future work in Section VI. Finally, we collected our experiments into a publicly available dataset for testing the validity of other localization or mapping methods with respect to variations in height.[1]

II. A METRIC OF MAGNETIC FIELD DIFFERENCE IN POSITIONING

In this section, we state the threshold that we will use in the rest of the paper for determining "significant" differences in the magnetic field with respect to height. This metric is motivated by two different applications of indoor positioning technology. First, we consider the use of indoor positioning technology to serve as an assistant to the blind and visually impaired (BVI). In a recent Federal Aviation Administration report, a requirement that BVI assistants position users to within two meters was proposed [21]. Using indoor positioning on smartphones has also been proposed to provide information to retailers regarding the effectiveness of certain displays and placement of products in stores [22]. Based on the average shelf space in US convenient stores, we set the requirement for this retail positioning application to be less than 0.2 meters on average [23]. A summary of scenarios and their positioning requirements is given in Table I.

[1]http://bretl.csl.illinois.edu/indoor-magnetic-positioning

Using Monte Carlo localization and Gaussian process regression on a portion of the MagPIE dataset, we find that disturbances above $1\ \mu T$ can cause our system to fail to meet requirements. Figure 2 shows the path considered in the MagPIE dataset [14]. The empirical cumulative distribution functions (CDFs) of the positioning error that results from different disturbances is shown in Figure 3. Therefore, in subsequent sections of this paper, we will look for differences in the magnetic field above $1\ \mu T$.

To produce this result, we apply a Monte Carlo localization method with 1000 particles and residual resampling. We map the magnitude of the magnetic field using the GPML toolbox and KISS-GP [24], [25]. We begin by assuming that the particles are initially distributed about the true starting point with a covariance equal to the positioning requirement. We also assume a constant velocity motion model of 1 meter per second. We believe this is a reasonable model for pedestrians. Based on prior research on pedestrian dead reckoning, we assume that the standard deviation of our motion model grows at 5.6% of the distance traveled [26]. Measurements are drawn from the same distribution as the map generated with GPML and KISS-GP. To test the impact of magnetic field disturbances on positioning, we assume that the differences in the magnetic field with respect to height are deterministic. Probabilistic differences occur due to sensor noise and other artifacts of experiment. We consider here the magnitude of the magnetic field rather than the entire magnetic vector. Therefore, we add a constant disturbance, d, to all of our measurements.

III. B-FIELD VARIATIONS WITH RESPECT TO A SINGLE MAGNETIC BEAM

In this section, we justify our study of the planar assumption by analytically considering a simple scenario: a single ferromagnetic beam. In particular, we will consider a rectangular beam of dimensions $2\ell \times 2h \times 2w$ that is homogeneously polarized in the x-direction (see Figure 4d). The solution for the magnetic field about this beam is given by Yang et al and is listed in Appendix A [27].

Based on experiments by Gozick et al, we choose the magnetic dipole moment to be $1.55 \times 10^3\ Am^2$ [12]. This produces a magnetic field of magnitude near $50\ \mu T$ half a meter away from the beam. We will consider the magnetic field for a beam that is $0.2\ m \times 3.9\ m \times 0.2\ m$, which is a typical floor to floor height of office buildings as suggested by the Council on Tall Buildings and Urban Habitat [28]. Contours of the magnitude of the magnetic field in the x-y plane are shown in Figures 4a, 4b, and 4c.

Horizontal lines on Figure 4 show the approximate heights of a Clearpath Jackal robot, a phone placed in one's pocket, a phone held in one's hand, and a phone held to one's ear. Given the position of a magnetometer (say Magnetometer 1), we find the difference in the magnetic field measured by a second magnetometer some distance, Δh, below Magnetometer 1. The thick, dashed, black lines in Figure 4 show the lines at which this difference in the measured magnitude of the magnetic field is equal to $1\ \mu T$: our previously stated threshold of

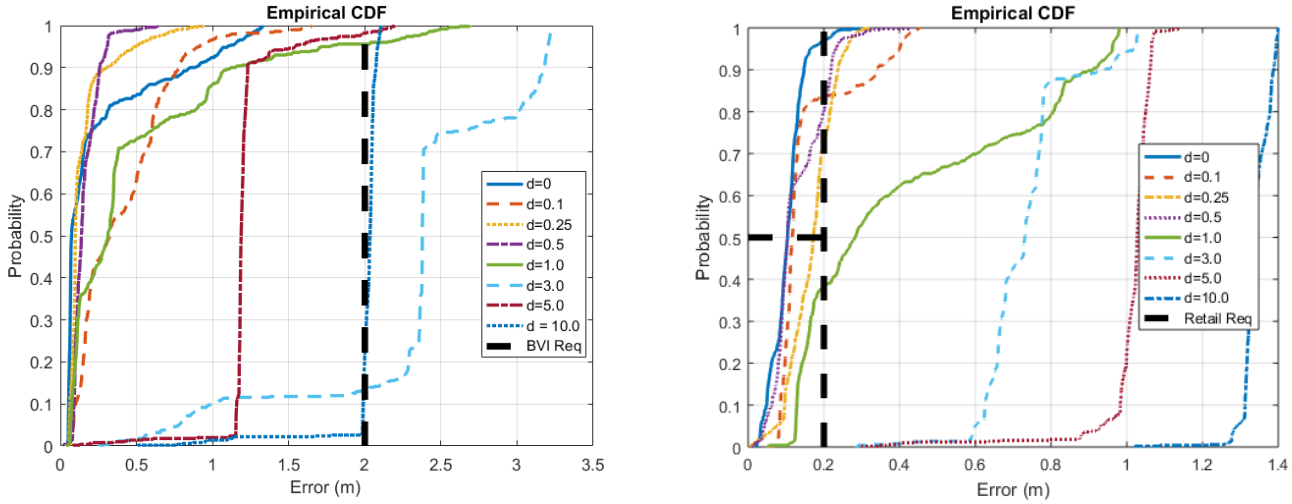

(a) Empirical cumulative distribution of error for BVI case.

(b) Empirical cumulative distribution of error for retail case.

Fig. 3. Empirical cumulative distribution functions of error for a simple Monte Carlo localization method for different degrees of constant magnetic field disturbance. For both BVI and retail scenarios, we would like to ensure this disturbance is less than 1 μT.

significance. Shaded regions are areas where the difference is greater than 1 μT. Figure 4a shows this threshold for a height difference of 0.0762 m, the approximate standard deviation of the heights of men and women. Figure 4b shows this threshold for a height of 0.30 m, which is the approximate height difference between an individual's phone when held in hand and in pocket. This is also approximately the 95% range in the heights of men and women. Finally, Figure 4c shows this threshold for a height difference of 0.75 m, which is the approximate height difference between an individual's phone when held to the ear and in pocket.

These results demonstrate that, even for the case of a single magnetic beam, differences in height can exceed our threshold value. This occurs as the difference in height (Δh) grows larger, as we move closer to the magnetic beam, and at lower heights (of Magnetometer 1).

IV. Experimental Methodology

We collect measurements of the magnetic field as well as the orientation and position of a Clearpath Jackal robot as it is manually driven in two buildings at the University of Illinois at Urbana-Champaign: a motion capture arena and inside the Materials Testing Facility. The first location was used due to the ease with which a system can be tested. The latter location is used for test because it better reflects one of the five types of buildings described in ISO/IEC 18305: a warehouse or factory. On top of the Jackal robot, we attach a rig of 20 three-axis magnetometers spaced three inches apart vertically. The magnetometers are connected to three Arduino Megas, which are in turn connected to the robot's main computer. Position and orientation measurements of the robot and its magnetometers are made in both buildings with a set of 24, OptiTrack Flex 3 motion capture cameras. The Jackal has many sensors included on-board the robot such as an inertial measurement unit, wheel encoders, etc. We also collect this data during our tests as well, though it is not critical to our experiments here. Figure 5 shows the robot and the attached rig on which magnetometers are mounted annotated with distance measurements. We follow motion capture calibration procedures provided by the manufacturer.

We use NXP MAG3110 magnetometers collecting at frequencies between 15 and 30 Hz to measure the magnetic field at all 20 heights. These three axis magnetometers were designed for use as an electronic compass and with location-based services. The magnetometer is reported to have a range of $\pm 1000\,\mu T$, a resolution of $0.10\,\mu T$, and noise down to $0.25\,\mu T$ root mean squared. However, during our own testing, we found that the NXP MAG3110 had higher noise than reported (about $0.52\,\mu T$). Allan deviation plots of these magnetometers show that each sensor had a different RMS noise and a rate random walk (see Figure 6). The magnetometers are calibrated together for hard and soft iron biases while attached to the robot. This is done outside and away from buildings. Hard iron and soft iron biases are estimated using the procedure described by Merayo et al [29]. This approach projects data used for calibration to the unit sphere. We therefore scale our result by the magnitude of the magnetic field at Urbana, Illinois as given by the International Geomagnetic Reference Field model: $52.811\,\mu T$. Because we calibrate the system outside and subsequently perform our tests indoors, we acknowledge several confounding factors may erroneously appear in our dataset. For example, magnetometer temperature sensitivity or hysteresis can introduce bias in our sensors. To help account for these factors, we apply least squares to our test data in order to estimate residual hard iron bias in our sensors. If we assume that we collect n test points, for magnetometer sensor measurements y_1 and y_2 we find a bias

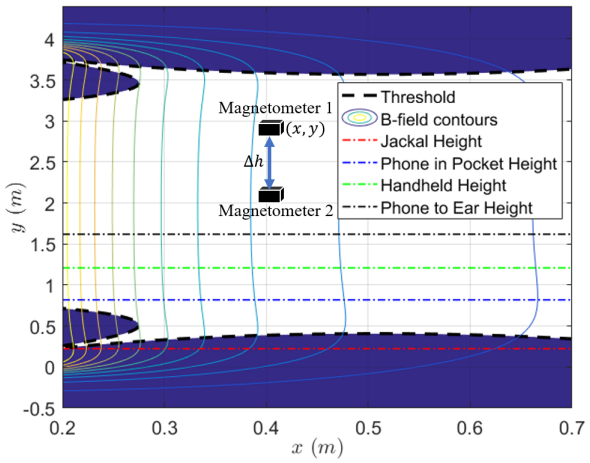

(a) Threshold given height difference of $0.0762\ m$.

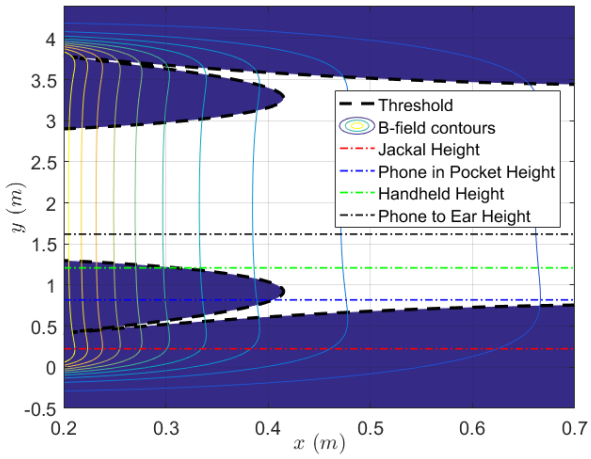

(b) Threshold given height difference of $0.30\ m$.

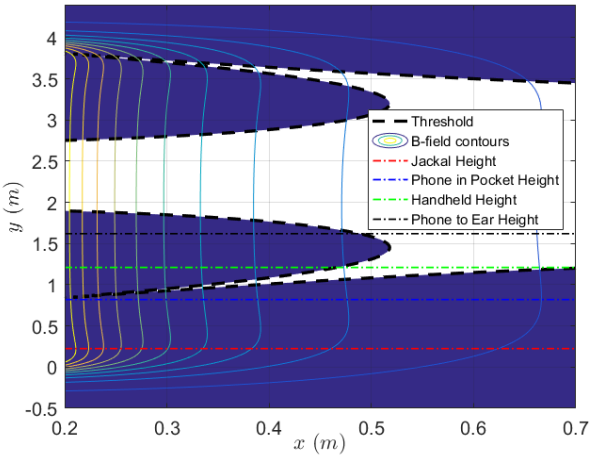

(c) Threshold given height difference of $0.75\ m$.

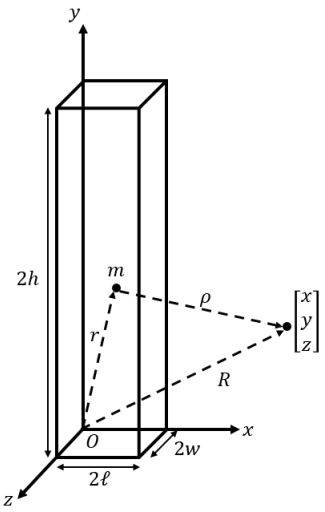

(d) Diagram of homogeneously polarized magnetic rectangular beam with dimensions $2\ell \times 2h \times 2w$ and dipole moment density m.

Fig. 4. The contours of the magnetic field magnitude for a $3.9\ m$ beam is shown along with the contour at which the difference between two magnetometers is $1\ \mu T$. The approximate height of a person with a phone in pocket, held in hand, held to the ear, and the height of a ground robot are displayed. The height variation in (a) is the standard deviation of heights of men and women. In (b) the height variation is approximately the difference between a phone in one's pocket and a phone in one's hand. Finally, (c) considers the distance between a phone to one's ear and a phone in one's pocket.

$\Delta_{1,2}$ that minimizes the following error

$$\Delta^*_{1,2} = \arg\min_{\Delta_{1,2}} \sum_{i=1}^{n} \|y_{1,i} - y_{2,i} - \Delta_{1,2}\|^2$$

and we then apply the following correction to our second sensor

$$\hat{y}_2 = y_2 + \Delta^*_{1,2}$$

where $\hat{y}_2$ is a corrected set of measurements. We perform this test relative to sensor number 11, which is near half the height of the test rig.

To establish that differences in the magnetic field exceed $1\ \mu T$ in a statistically significant way, we (1) produce maps with Gaussian process regression (GPR) for each magnetometer and (2) conduct an inequality test between two different Gaussian process regressions. Since we produce maps with GPR, at a given height we estimate

$$\boldsymbol{f}(x) \sim \mathcal{GP}\left(\mu(x), \hat{K}(x, x')\right)$$
$$y = f(x) + \epsilon, \qquad \mathcal{N}(0, \sigma_n^2)$$

where $\boldsymbol{f}$ is the estimated magnetic field magnitude described as a Gaussian process with a mean μ and covariance $\hat{K}$. All of these variables are dependent on a two dimensional position x. The predicted measurements made by the magnetometer y involve the Gaussian process itself plus normally distributed noise with variance σ_n^2. Our test is a modified version of the equality tests between two GPRs presented by Benavoli and Mangili [30]. Given two Gaussian process regressions $\boldsymbol{f}_1$ and $\boldsymbol{f}_2$ with mean functions μ_1 and μ_2 and covariance

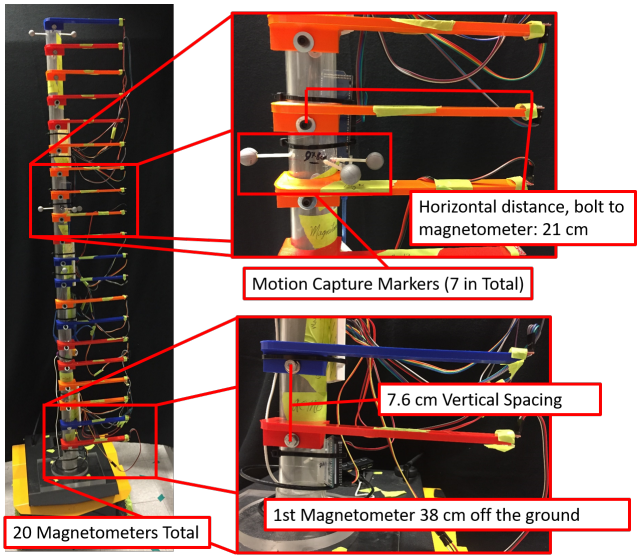

Fig. 5. The Clearpath Jackal robot along with the experimental rig. An NXP MAG3110 is attached to the end of each level. Several important dimensions are also displayed.

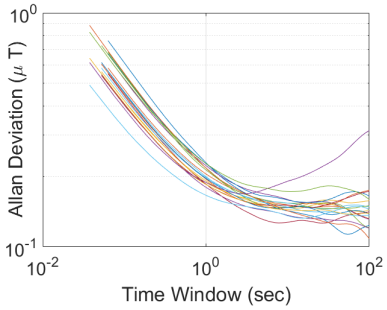

Fig. 6. Allan deviation plots for our 20 magnetometers show that our sensors have different RMS noise and rate random walk.

functions $\hat{K}_1$ and $\hat{K}_2$, the difference $\Delta \boldsymbol{f} = \boldsymbol{f}_1 - \boldsymbol{f}_2$ is also a Gaussian process. The Gaussian process $\Delta \boldsymbol{f}$ has mean $\Delta\mu = \mu_1 - \mu_2$ and covariance $\hat{K}_\Delta = \hat{K}_1 + \hat{K}_2$. To test if the difference between the maps of $\boldsymbol{f}_1$ and $\boldsymbol{f}_2$ are not equal, we first minimize the difference $\Delta\mu$ at a test point i according to the rule (shown in Figure 7)

$$\begin{aligned} \Delta\mu_i &= \mu_1 - \mu_2 - d \\ \text{where } d &= -1 \qquad \text{if } \mu_1 - \mu_2 < -1 \\ d &= \mu_1 - \mu_2 \quad \text{if } -1 \leq \mu_1 - \mu_2 \leq 1 \\ d &= 1 \qquad \text{if } \mu_1 - \mu_2 > 1. \end{aligned}$$

If for a test point i, our revised difference $\Delta\mu_i$ and variance $\hat{K}_\Delta$ satisfies the condition

$$\frac{\Delta\mu_i^2}{\hat{K}_\Delta} > \chi_1^2(\alpha) \tag{1}$$

where $\chi_1^2(\alpha)$ is the value of the χ^2 CDF for one degree of freedom at value α, then we can be confident with degree α that the difference in the magnitude of the magnetic field at

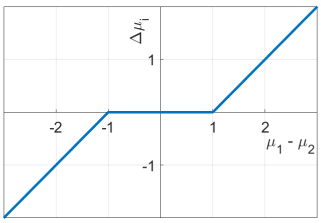

Fig. 7. Minimized difference $\Delta\mu_i$ with respect to actual difference $\mu_1 - \mu_2$.

the test point is greater than 1 μT. For this work, we choose an α of 0.95.

A test was conducted to verify that motors running on the Jackal robot did not produce a magnetic field that was noticeably measured by the magnetometers used in this experiment. To conduct this test, we first sat the robot still with no motors running and then had the robot spin its wheels (while propped up to remain still) at its maximum rotations per minute. We then compared the mean magnetic field measured by the magnetometer closest to the motors in these two cases. We found that the difference in the mean magnitude of the magnetic field for these two cases is less than 5 nT, which is far less than the sensitivity of the MAG3110 magnetometer.

Our methodology conservatively estimates differences in the magnetic field due to our use of least squares to estimate residual hard iron bias offsets. Despite this, it is worth acknowledging several remaining confounding factors that may influence our results. A variety of factors influence the measurements taken by the MAG3110 sensor, which is a magnetoresistive device. These factors include hysteresis with respect to the applied magnetic field, temperature sensitivity, measurement nonlinearity, sensor die-to-package misalignment, and sensor noise rate random walk. The degree to which these factors influence our results, however, may be categorized into at least the following two notions. First is soft iron bias error. We calibrate our system outside for soft and hard iron bias, however, our additional least square correction only attempts to address additional hard iron bias errors. We do not correct any additional soft iron bias errors that may appear during our tests. Second is temporal changes in hard iron bias. We calibrate our magnetometers prior to test and apply least squares on our test data as a single batch. If any of the factors above cause the hard iron bias to change with time, then it may act as a confounding factor in our experiment.

V. Experimental Evaluation

We evaluate the magnetic field by generating GPR maps of the two buildings. Due to the size of our dataset, we map the magnitude of the magnetic field with the GPML toolbox and KISS-GP as we did in Section II. Using a squared exponential kernel with automatic relevance determination, hyperparameters for the characteristic length scale, sensor noise (σ_n in Section II), signal noise, and a constant non-zero mean, we optimize the negative marginal log likelihood using LBFGS. KISS-GP applies structured kernel interpolation to an inducing point GPR method. In this case, we apply

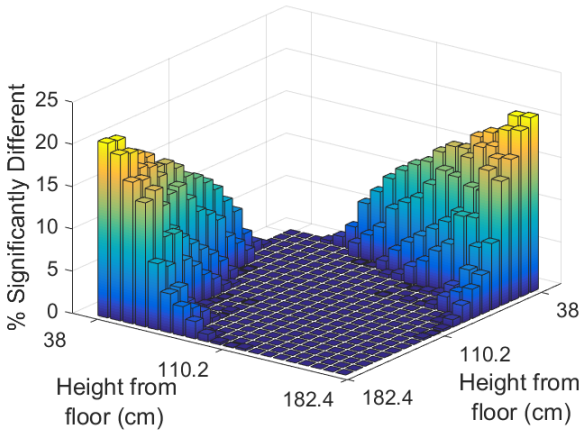

(a) Percent of significantly different test points comparing magnetic magnitude of maps generated from a pair of sensors in our motion capture arena (bar plot).

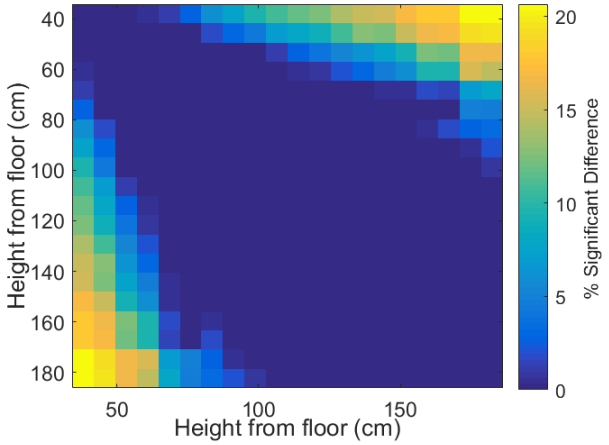

(b) Percent of significantly different test points comparing magnetic magnitude of maps generated from a pair of sensors in our motion capture arena (heat map).

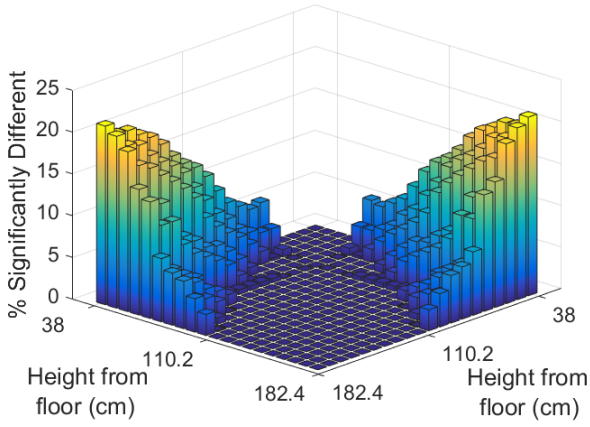

(c) Percent of significantly different test points comparing magnetic magnitude of maps generated from a pair of sensors in the Materials Testing Facility (bar plot).

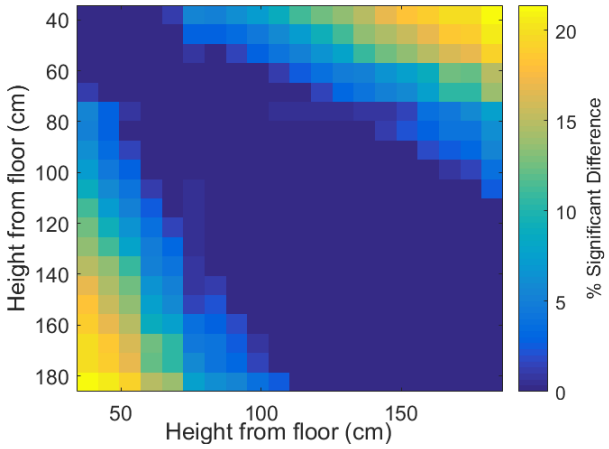

(d) Percent of significantly different test points comparing magnetic magnitude of maps generated from a pair of sensors in the Materials Testing Facility (heat map).

Fig. 8. The percent of test points that have significantly different magnetic field norms between pairs of magnetometers. We can see that the further away a pair of magnetometers are from eachother, the higher the percent of test points are different. Variations of the magnetic field with respect to height are also greater the closer to the floor a magnetometer is.

this interpolation to the fully independent training conditional (FITC) method with a grid of 1600×1600 inducing points. Ninety percent of our data is used for training the GPR map. Ten percent of our data is used for our statistical tests and for evaluating the quality of the GPR map. Standard metrics for measuring the quality of a GPR map include the standardized mean square error (SMSE) and mean standardized log loss (MSLL) [31]. Both metrics are presented for each map in Table II.

Figure 8 shows the percent of test points wherein the difference in the magnitude of the magnetic field between a pair of sensors are found to be statistically significant. Figures 8a and 8c show the results as a 3D bar plot where the x and y axes correspond to the numbers of the magnetometers that are to be compared and the z-axis is the percent of test points that were determined to be statistically significant. The same results for the motion capture arena and the Materials Testing Facility are shown in Figures 8b and 8d as heat maps. The color corresponds the the percent of test points that were determined to be statistically significant. Here, it can clearly be seen that the further sensors are separated with respect to height, the higher the percent of points that are significantly different. Moreover, magnetometers closer to the floor in both buildings appear to experience greater variations in the magnetic field with respect to height than sensors near the top of the rig. This is a predictable result using the model of a magnetic metal beam considered in Section III. Finally, we see that variations with respect to height are larger in the Materials Testing Facility than they are in the motion capture arena.

Points wherein significant differences between measure-

TABLE II
STANDARDIZED MEAN SQUARED ERROR AND MEAN STANDARDIZED LOG LOSS FOR GPR MAPS

Mag. Number	Magnetometer Height (cm)	Motion Capture Arena		Materials Testing Facility	
		SMSE	MSLL	SMSE	MSLL
1	182.4	0.1911	-0.6324	0.1147	-0.8443
2	174.8	0.1515	-0.6999	0.05734	-0.9893
3	167.2	0.1226	-0.6928	0.03916	-1.0663
4	159.6	0.1636	-0.6490	0.04388	-1.0508
5	152	0.1950	-0.5934	0.04532	-1.0593
6	144.4	0.1619	-0.6158	0.03704	-1.0645
7	136.8	0.1574	-0.6430	0.02788	-1.1324
8	129.2	0.1966	-0.5857	0.03193	-1.1177
9	121.6	0.1877	-0.5961	0.02550	-1.1489
10	114	0.1585	-0.6736	0.01999	-1.1847
11	106.4	0.1356	-0.6790	0.01641	-1.2102
12	98.8	0.2066	-0.6259	0.02244	-1.1684
13	91.2	0.1140	-0.7498	0.01169	-1.2167
14	83.6	0.1041	-0.7971	0.01220	-1.2141
15	76	0.1148	-0.7543	0.03292	-1.0211
16	68.4	0.1562	-0.6748	0.01792	-1.1793
17	60.8	0.08813	-0.8697	0.009583	-1.1750
18	53.2	0.08179	-0.8413	0.01183	-1.1955
19	45.6	0.09117	-0.8412	0.01259	-1.1595
20	38	0.05328	-0.9578	0.01037	-1.1875

ments are found are not scattered evenly about the Materials Testing Facility and the motion capture arena. Rather they tend to occur only in certain areas of the mapped space. Presumably these areas are near strong magnetic sources in the floor of the buildings. Figure 9 shows all the test points used in the motion capture arena and the Materials Testing Facility. At these plots, we compare estimated measurements from Magnetometer 10 and Magnetometer 20. The former magnetometer is near the height at which a smart phone might be held in one's hand. The latter magnetometer is closest to our robot. Test points wherein anticipated measurements between these two sensors are significantly different are shown as red circles.

VI. CONCLUSION

In this work, we sought to test the hypothesis that the magnetic field inside a building can vary significantly as a function of height. We do this by comparing the measurements of magnetometers in two different buildings at 20 different heights. We found that up to 20% of points in these two buildings had pairwise differences greater than $1\,\mu T$. We confirmed our hypothesis analytically for a single magnetic beam. This variation in height appears to be greater near the floor of the building than it is near the height of an average man or woman.

The possibility of positioning pedestrians and robots in the presence of a magnetic field that may vary with height may have several implications. First, because differences in the magnetic field seem to be concentrated in certain regions of a building (see Figure 9), it may be wise to include outlier rejection as part of magnetic field-based localization schemes. Alternatively, it may be help to classify the position of the phone (held in hand, in pocket, etc.) prior to using magnetic field data for positioning. Finally, it may be informative to include height variations as part of standardized test and evaluation procedures for magnetometer-based indoor positioning systems.

Future work consists of evaluating the magnetic field for additional structures described in ISO/IEC 18305. Changes in the direction of the magnetic field as well as its magnitude should also be considered. Finally, an important expansion to this work would be to experimentally show cases wherein the planar assumption is reasonable.

APPENDIX A
FIELD OF A MAGNETIC BEAM

The equations of the magnetic field for a rectangular beam of size $2\ell \times 2h \times 2w$ that is homogeneously polarized in the x-direction (see Figure 4d) were stated by Yang et al [27]. These equations are

$$\begin{aligned} B_x =& -\frac{\mu_0 m}{4\pi}[F_1(-x,y,z) + F_1(-x,y,-z) \\ &+ F_1(-x,-y,z) + F_1(-x,-y,-z) + F_1(x,y,z) \\ &+ F_1(x,y,-z) + F_1(x,-y,z) + F_1(x,-y,-z)] \\ B_y =& \frac{\mu_0 m}{4\pi} \ln\left(\frac{F_2(-x,-y,z)F_2(x,y,z)}{F_2(-x,y,z)F_2(x,-y,z)}\right) \\ B_z =& \frac{\mu_0 m}{4\pi} \ln\left(\frac{F_2(-x,-z,y)F_2(x,z,y)}{F_2(-x,z,y)F_2(x,-z,y)}\right) \end{aligned}$$

where μ_0 is the permeability of free space, m is the magnitude of the magnetic dipole moment, the magnetic field vector is $\boldsymbol{B} = \begin{bmatrix} B_x & B_y & B_z \end{bmatrix}^T$, and

$$F_1(x,y,z) = \tan^{-1}\left(\frac{(h+y)(w+z)}{(\ell+x)\sqrt{(\ell+x)^2+(h+y)^2+(w+z)^2}}\right)$$

$$F_2(x,y,z) = \frac{\sqrt{(\ell+x)^2+(h+y)^2+(w-z)^2}+w-z}{\sqrt{(\ell+x)^2+(h+y)^2+(w+z)^2}-w-z}.$$

ACKNOWLEDGMENT

This work was supported by the National Science Foundation Grant No. 14-46765 and 14-27111. The authors would like to thank Scott D. Zelman for help constructing portions of our experimental rig.

REFERENCES

[1] S. A. Rahok, Y. Shikanai, and K. Ozaki, "Navigation Using an Environmental Magnetic Field for Outdoor Autonomous Mobile Robots," *Advanced Robotics*, vol. 25, no. 13-14, pp. 1751–1771, 2011.

[2] K. P. Subbu, B. Gozick, and R. Dantu, "LocateMe: Magnetic-fields-based Indoor Localization Using Smartphones," *ACM Trans. Intell. Syst. Technol.*, vol. 4, no. 4, pp. 73:1–73:27, Oct. 2013.

[3] J. Chung, M. Donahoe, C. Schmandt, I.-J. Kim, P. Razavai, and M. Wiseman, "Indoor Location Sensing Using Geo-magnetism," in *Int. Conf. Mobile Systems, Applications, and Services*, ser. MobiSys '11. New York, NY, USA: ACM, 2011, pp. 141–154.

[4] C. Gao and R. Harle, "MSGD: Scalable back-end for indoor magnetic field-based GraphSLAM," in *Int. Conf. Robotics and Automation (ICRA)*, May 2017, pp. 3855–3862.

[5] J. Haverinen and A. Kemppainen, "Global indoor self-localization based on the ambient magnetic field," *Robotics and Autonomous Systems*, vol. 57, no. 10, pp. 1028 – 1035, 2009.

[6] E. L. Grand and S. Thrun, "3-Axis Magnetic Field Mapping and Fusion for Indoor Localization," in *Int. Conf. Multisensor Fusion and Integration for Intelligent Systems (MFI)*, Sept 2012, pp. 358–364.

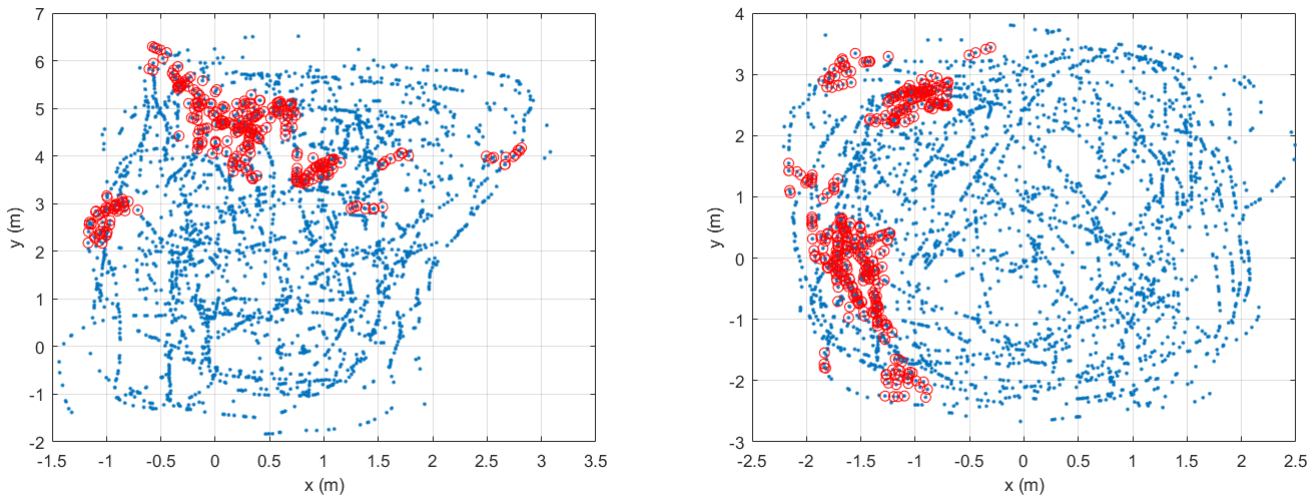

(a) Materials Testing Facility.

(b) Motion Capture Arena.

Fig. 9. Points we use to test the difference between measurements from Magnetometer 10 and 20 are shown for our two buildings. Points where differences between the magnetic field at these two heights are statistically significant are shown as red circles.

[7] B. Kim and S. H. Kong, "A Novel Indoor Positioning Technique Using Magnetic Fingerprint Difference," *IEEE Trans. Instrum. Meas.*, vol. 65, no. 9, pp. 2035–2045, Sept 2016.

[8] X. Wang, C. Zhang, F. Liu, Y. Dong, and X. Xu, "Exponentially Weighted Particle Filter for Simultaneous Localization and Mapping Based on Magnetic Field Measurements," *IEEE Trans. Instrum. Meas.*, vol. 66, no. 7, pp. 1658–1667, July 2017.

[9] N. Lee and D. Han, "Magnetic indoor positioning system using deep neural network," in *Int. Conf. Indoor Positioning and Indoor Navigation*, Sept 2017, pp. 1–8.

[10] R. Montoliu, J. Torres-Sospedra, and O. Belmonte, "Magnetic Field Based Indoor Positioning using the Bag of Words Paradigm," in *Int. Conf. Indoor Positioning and Indoor Navigation*, Oct 2016, pp. 1–7.

[11] D. Carrillo, V. Moreno, B. Ubeda, and A. F. Skarmeta, "MagicFinger: 3D Magnetic Fingerprints for Indoor Location," *Sensors*, vol. 15, no. 7, pp. 17 168–17 194, 2015.

[12] B. Gozick, K. P. Subbu, R. Dantu, and T. Maeshiro, "Magnetic Maps for Indoor Navigation," *IEEE Trans. Instrum. Meas.*, vol. 60, no. 12, pp. 3883–3891, Dec 2011.

[13] N. Moayeri, M. O. Ergin, F. Lemic, V. Handziski, and A. Wolisz, "PerfLoc (Part 1): An extensive data repository for development of smartphone indoor localization apps," in *Int. Symp. on Personal, Indoor, and Mobile Radio Communications*, Sept 2016, pp. 1–7.

[14] D. Hanley, A. B. Faustino, S. D. Zelman, D. A. Degenhardt, and T. Bretl, "MagPIE: A Dataset for Indoor Positioning with Magnetic Anomalies," in *Int. Conf. Indoor Positioning and Indoor Navigation*, Sept 2017, pp. 1–8.

[15] D. Lymberopoulos, J. Liu, X. Yang, R. R. Choudhury, V. Handziski, and S. Sen, "A Realistic Evaluation and Comparison of Indoor Location Technologies: Experiences and Lessons Learned," in *Int. Conf. Information Processing in Sensor Networks*, ser. IPSN '15. New York, NY, USA: ACM, 2015, pp. 178–189.

[16] "Information Technology – Real Time Locating Systems – Test and Evaluation of Localization and Tracking Systems," International Organization for Standardization, Geneva, CH, Standard, 2016.

[17] N. Akai and K. Ozaki, "3D magnetic field mapping in large-scale indoor environment using measurement robot and Gaussian processes," in *Int. Conf. Indoor Positioning and Indoor Navigation*, Sept 2017, pp. 1–7.

[18] K. Yamazaki, K. Kato, K. Ono, H. Saegusa, K. Tokunaga, Y. Iida, S. Yamamoto, K. Ashiho, K. Fujiwara, and N. Takahashi, "Analysis of magnetic disturbance due to buildings," *IEEE Trans. Magn.*, vol. 39, no. 5, pp. 3226–3228, Sept 2003.

[19] D. Caruso, A. Eudes, M. Sanfourche, D. Vissiere, and G. le Besnerais, "An inverse square root filter for robust indoor/outdoor magneto-visual-inertial odometry," in *Int. Conf. Indoor Positioning and Indoor Navigation*, Sept 2017, pp. 1–8.

[20] "Advance Data from Vital and Health Statistics: Numbers 1-10," National Center for Health Statistics, Hyattsville, MD, Tech. Rep. 16(1), May 1989, DHHS Publication No. (PHS) 89-1860.

[21] G. W. Legge, C. Downey, N. A. Giudice, and B. S. Tjan, "Indoor Airport Wayfinding for Blind and Visually Impaired Travelers," Federal Aviation Administration Office of Airport Safety and Standards, Washington, DC, Tech. Rep. DOT/FAA/TC-TN16/54, December 2016.

[22] K. Kanagu, K. Tsubouchi, and N. Nishio, "Colorful PDR: Colorizing PDR with Shopping Context in Walking," in *Int. Conf. Indoor Positioning and Indoor Navigation*, Sapporo, Japan, September 2017.

[23] C. Chun, T. M. Schmit, D. Dong, and H. M. Kaiser, "Economic Evaluation of Shelf-Space Management in Grocery Stores," *Agribusiness*, vol. 23, no. 4, pp. 583–597, October 2007.

[24] C. E. Rasmussen and H. Nickisch, "Gaussian Processes for Machine Learning (GPML) Toolbox," *Journal of Machine Learning Research*, vol. 11, pp. 3011–3015, November 2010.

[25] A. G. Wilson and H. Nickisch, "Kernel Interpolation for Scalable Structured Gaussian Processes (KISS-GP)," in *Int. Conf, on Machine Learning*, ser. ICML'15, 2015, pp. 1775–1784.

[26] R. Harle, "A survey of indoor inertial positioning systems for pedestrians," *IEEE Commun. Surveys Tuts.*, vol. 15, no. 3, pp. 1281–1293, 2013.

[27] Z. J. Yang, T. H. Johansen, H. Bratsberg, G. Helgesen, and A. T. Skjeltorp, "Potential and force between a magnet and a bulk $Y_1Ba_2Cu_3O_{7-\delta}$ superconductor studied by a mechanical pendulum," *Superconductor Sci. and Technol.*, vol. 3, no. 12, p. 591, 1990.

[28] *CTBUH Tall Building Height Calculator*, Council on Tall Buildings and Urban Habitat. [Online]. Available: http://www.ctbuh.org/LinkClick.aspx?fileticket=s4SVxV%2fruCM%3d&tabid=1007&language=en-GB

[29] J. M. G. Merayo, P. Brauer, F. Primdahl, J. R. Petersen, and O. V. Nielsen, "Scalar calibration of vector magnetometers," *Measurement Sci. and Technol.*, vol. 11, no. 2, p. 120, 2000.

[30] A. Benavoli and F. Mangili, "Gaussian Processes for Bayesian hypothesis tests on regression functions," in *Int. Conf. Artificial Intelligence and Statistics*, ser. Proceedings of Machine Learning Research, G. Lebanon and S. V. N. Vishwanathan, Eds., vol. 38, San Diego, California, USA, 09–12 May 2015, pp. 74–82.

[31] C. E. Rasmussen and C. K. I. Williams, *Gaussian Processes for Machine Learning*, ser. Adaptive Computation and Machine Learning, T. Dietterich, Ed. Cambridge, MA: The MIT Press, 2006.